Enhancement of InGaN Quantum Well Photoluminescence in a Tamm Metal/Porous-DBR Micro-Cavity

Andrei Sarua, Jon Pugh, Edmund Harbord, and Martin Cryan, *Senior Member, IEEE*

***Abstract*—Vertical cavity surface emitting lasers (VCSEL) are of great interest for photonic and telecom applications, however challenges in fabrication of efficient VSCEL GaN devices are yet to be resolved. In this work we present a study of micro-photoluminescence (PL) emission from a novel InGaN quantum well (QW) emitting structure with integrated micro-cavity, which can be used for VCSEL applications. The micro-cavity exhibiting Tamm plasmon optical states is formed by a porous GaN distributed Bragg reflector (DBR) bottom mirror and top plasmonic silver metal mirror. Results of PL, Fourier imaging spectroscopy and finite-difference time-domain simulations are presented and discussed. An estimated 8.5 times enhancement of QW PL intensity at around 480–500 nm and a red-shift of QW peak emission is attributed to the Tamm plasmon resonance in the cavity at around 514 nm.**

***Index Terms*—Distributed Bragg reflector, Tamm plasmon, porous GaN, InGaN, quantum well, laser, LED, quantum well, VCSEL.**

I. Introduction

THERE has been remarkable progress in III-V nitride technology across various semiconductor device markets from solid-state lighting to the state-of-the-art RF and power devices over the past two decades [1], [2]. However, despite some significant effort in fabrication of various light emitting devices, there has been one notable gap in the GaN device technology – vertical cavity surface emitting laser (VCSEL) devices. While various UV and visible laser diode structures based on GaN and its alloys were proposed and manufactured [1], [2], [3], in contrast to the GaAs family, successful commercial VCSEL structures based on GaN are yet to be demonstrated. VCSEL devices have a broad range of applications and are common in the telecom and display applications, due to their planar structure, discrete pixel configuration and compact cavity size. There have been several research demonstrations for GaN based VCSEL structures in the scientific literature, mainly in the blue emitting region [4], [5]. Many challenges associated with the growth and fabrication of GaN VCSEL structures still remain, especially for the green-yellow-red parts of the visible spectrum [4], [5], [6], [7], [8]. While vertically emitting diode structures are common for GaN LED markets and are available commercially, VCSELs require an optical micro-cavity formed by a pair of distributed Bragg reflector (DBR) mirrors made of several pairs, on order of 10 or more, of ultra-thin layers with modulated index of refraction, n [3], [4], [8], [9]. In addition, a challenge remains to maintain good p- and n-type electrical conductivity vertically throughout the device, needed to reduce series resistance for the electrically pumped laser devices. In particular, this relates to the DBR layers in the conventional VCSEL structure, which need to conduct electric current into the active area of the cavity, i.e., single or multiple quantum well (SQW and MQW) region, and be efficient in simultaneously confining light in the micro-cavity. An optimal way to create such stacks of electrically conductive and crack free layers using GaN and related materials is yet to be realised, especially for the p-type contact region. Many successful approaches so far are based on the growth of a hybrid structure, where the bottom n-type DBR is formed by pairs of alternating Al/In fraction (Al/In)GaN and GaN, and then a top DBR mirror is formed in a separate fabrication step on the p-type GaN and transparent indium tin oxide (ITO) contact layer using a stack of dielectric non-conductive materials e.g., SiN or SiO2 [4], [5], [8], however, this generally makes device fabrication complicated. For the bottom DBR, a large number of alternating (Al/In)GaN and GaN pairs is required in order to achieve a high reflectivity, as the refractive index contrast between AlGaN and GaN is intrinsically small. [4] Furthermore, given the large lattice mismatch [10], such a DBR leads to a number of issues for further device layers growth on its top, such as cracking, rough surface, and extra dislocations.

In this work, we propose a novel way to form a lasing micro-cavity (MC) for a GaN based VCSEL device, by combining recent progress in the fabrication of highly reflective porous-GaN/GaN DBR structures [6], [7], [8], [9], [10], [11] and a so-called Tamm plasmons [12], [13] in which photonic surface state is formed in the cavity between a DBR mirror

Manuscript received 22 June 2023; revised 3 August 2023; accepted 15 August 2023. Date of publication 18 August 2023; date of current version 4 September 2023. This work was supported by EPSRC under Grant EP/M015181/1. *(Corresponding author: Andrei Sarua.)*

Andrei Sarua is with the Center for Device Thermography and Reliability, School of Physics, University of Bristol, BS8 1TL Bristol, U.K. (e-mail: a.sarua@bristol.ac.uk).

Jon Pugh and Martin Cryan are with the Department of Electrical and Electronic Engineering, Photonics and Quantum Group, University of Bristol, BS8 1UB Bristol, U.K. (e-mail: jon.pugh@bristol.ac.uk; m.cryan@bristol.ac.uk).

Edmund Harbord is with the Quantum Engineering Technology Labs, H. H. Wills Physics Laboratory, and Department of Electrical and Electronic Engineering, University of Bristol, BS8 1FD Bristol, U.K. (e-mail: edmund.hardord@bristol.ac.uk).

Digital Object Identifier 10.1109/JPHOT.2023.3306344

and a thin metal film [11], [14], [15], [16], [17], [18]. Such porous-DBRs have an advantage of a very high refractive index contrast between GaN and porous-GaN layers in a stack, due to air filling the pores and are nearly stress free due to lack of lattice constant mismatch. This minimises the total layer thickness required to achieve a high, >0.99 reflectivity stop-band in the optical cavity[17], improving series resistance and removing built-in stress and cracking associated with growth of stacks of multiple AlGaN/GaN or InGaN/GaN layers. Metal layer based Tamm plasmon optical states were successfully demonstrated for e.g., GaAs vertically emitting lasers [19] and for other light emitting devices [17], [20]. Metal plasmonic layers as top mirrors in a VCSEL have an advantage of maintaining electrical conductivity and their properties can be tailored to enhance the local electric field and hence the emission properties of quantum wells, e.g., via Tamm resonance and Purcell effect [21]. Here, we explore enhancement of optical photoluminescence properties of the InGaN MQW emitting structure confined in a vertical hybrid MC formed by a bottom porous-GaN DBR structure and top silver metal plasmonic contact, which can form a basis for an electrically pumped GaN VCSEL.

II. Experimental Details

The InGaN quantum well sample with a DBR structure was grown on a (0001) sapphire substrate using a low-pressure metal-organic-vapour phase epitaxy (MOVPE) system via a standard two-step growth method. A low-temperature 25 nm GaN nucleation layer is deposited first, followed by a 1.5 μm GaN layer grown at 1100 °C, see in Fig. 1(a). The basis for the DBR structure is formed then by a growth of 11 pairs of unintentionally doped (UID) GaN and heavily silicon doped n-GaN layers, with the Si doping level of $\sim 10^{19}$ cm^{-3}. The thicknesses of the UID and the n-GaN layers in each pair are 50 nm and 65 nm, respectively. A micro-cavity and emitting structure is grown, which consists of a 54 nm UID-GaN layer, 3 pairs of InGaN/GaN multiple quantum wells (MQW) and a further 54 nm undoped GaN layer shown in Fig. 1(b). The nominal indium composition of the InGaN MQWs is around 18%, while the QW and the GaN barrier thicknesses are 2.5 nm and 10 nm, respectively. The porous DBR structure of total thickness of around 1.215 μm is then fabricated over selected sample area by an electrochemical etching of 11 pairs of undoped/n-GaN layers shown in Fig. 1(a) and (c) as described in detail elsewhere [10], [22], following methods of Zhang et al. [6] and Zhu et al. [23]. Cross-sectional scanning electron microscopy (SEM) image of the porous-DBR and top micro-cavity is shown in Fig. 1(d). Finally, the 25 nm thick silver and 20 nm thick protective SiO_2 coating, to avoid environmental deterioration of metal contact, were deposited onto the surface using e-beam evaporator and some areas of the sample were masked to leave the native surface exposed, see Fig. 1(c).

Micro-photoluminescence measurements of the InGaN multiple quantum well structure were performed using a Renishaw NUV RM2000 spectrometer. The 325 nm light from a CW Kimmon HeCd laser was focused on the sample using 40x objective lens (NA = 0.47) in a spot of about 1–2 μm diameter

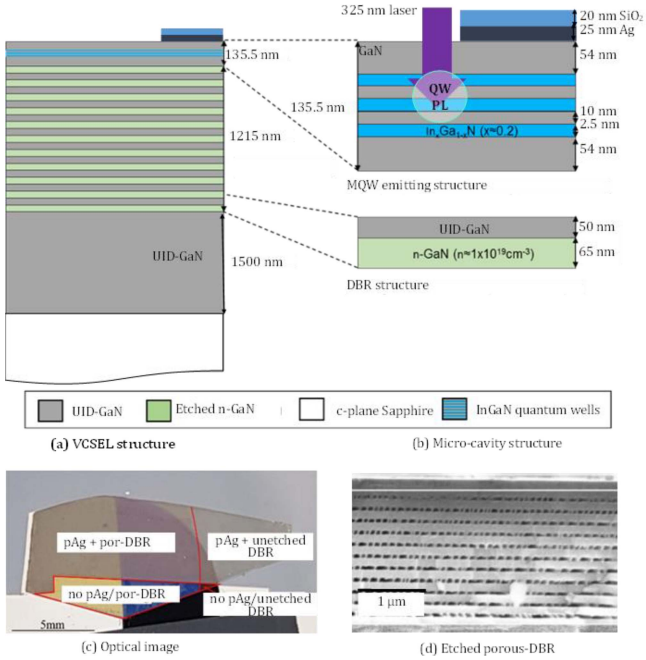

Fig. 1. (a) GaN VCSEL structure grown for this study. (b) Multiple quantum well (MQW) and micro-cavity structure. Legend shows materials used for the structure: unintentionally doped UID-GaN, Si doped n-GaN or etched porous n-GaN, c-plane oriented sapphire and InGaN quantum wells. Nominal layer thicknesses for protected silver layer (pAg) and other layers in the structure are shown. Laser excitation at 325 nm and QW PL are shown schematically as illustration. (c) Optical image of the sample with four characteristic areas: uncoated (no pAg) as-grown with unetched DBR, uncoated with etched porous DBR (por-DBR), pAg-coated with unetched DBR, and pAg-coated with porous DBR. Red lines show approximate area borders. (d) SEM image of the cross-section of the porous DBR region after electrochemical etching.

and total power was limited to about 0.3 mW to avoid local heating effects. The sample was mounted on the microscope XY stage with 1 μm step resolution. The measurements were conducted at room temperature at multiple locations on the sample. Sample reflectivity in the spectral range from 400–600 nm from different areas was characterised using a tungsten lamp white light source and a Fourier imaging spectroscopy (FIS) set-up with a high 0.9 NA optical objective as described in [11]. Simulations of the optical properties of all layers including porous-GaN were performed using a Lumerical finite-difference time-domain (FDTD) code. Details of FIS measurements and simulations are described elsewhere [11].

III. Results and Discussion

Fig. 2 shows the PL results obtained from the four different areas on the sample: (a) Uncoated as-grown, (b) Etched porous-DBR areas, (c) Coated with protected silver (pAg) layer as-grown and (d) Protected silver (pAg) layer with etched porous-DBR regions. As intensity of the PL signal varied over the selected areas, as shown by examples of spectra for the same area, solid lines in Fig. 2(a)–(d), it was necessary to average the spectra recorded, and those averaged spectra are also plotted alongside, see dashed lines in Fig. 2(a)–(d). In common, all

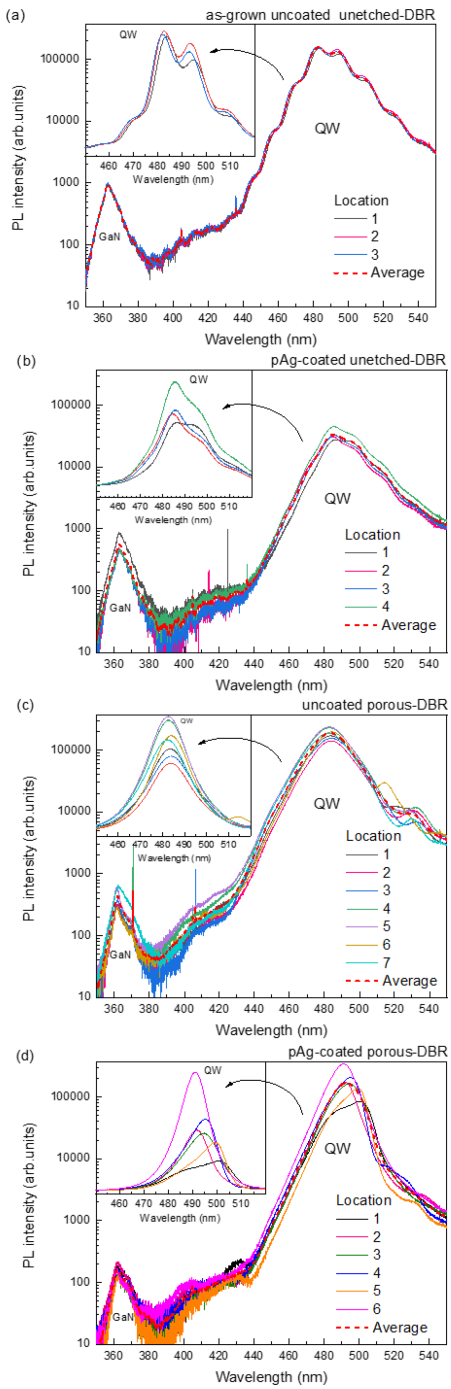

Fig. 2. Photoluminescence spectra of (a) as-grown uncoated, (b) protected silver (pAg) coated as-grown, (c) uncoated etched porous-DBR and (d) protected silver coated etched porous-DBR regions. Note, the vertical axis scale for PL intensity is identical in all graphs and plotted on the logarithmic scale. Plotted for each graph: a typical measured PL signal from multiple locations (solid lines) and an average spectrum (dashed red lines). The insets show QW PL region in detail on the linear intensity scale for clarity.

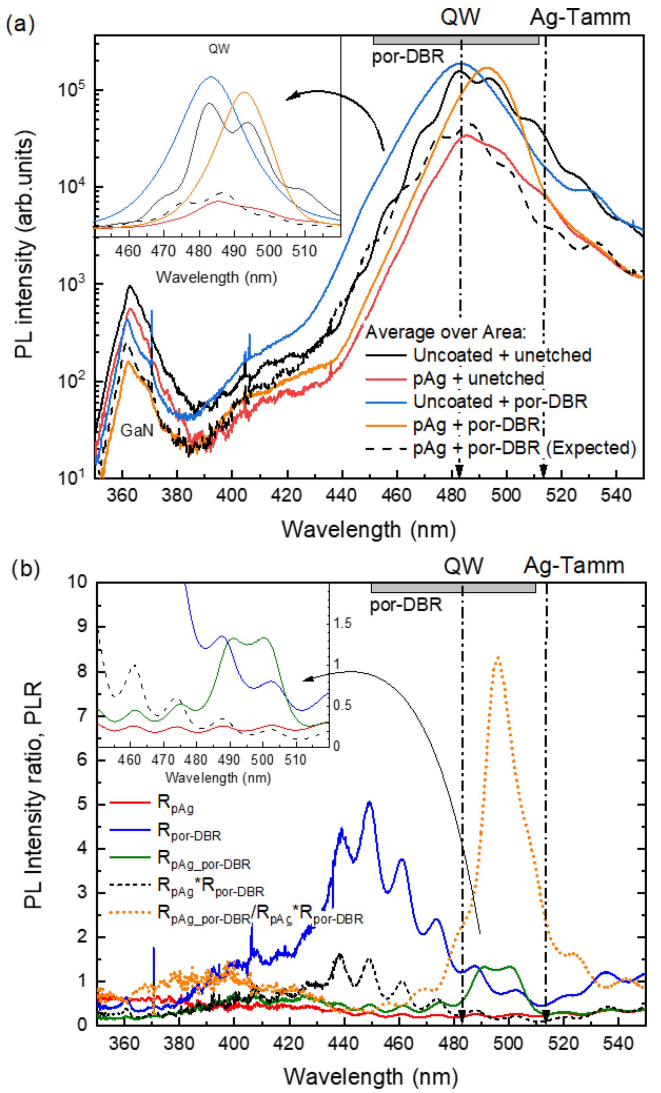

Fig. 3. (a) Average PL spectra for the specified area on the sample (solid lines). Expected spectrum for the effect of protected silver mirror and porous-DBR (dashed line) to compare with actual PL spectrum for this area (see Section III-D for definitions). All data are plotted on the log scale. (b) Ratio of average PL intensities (*PLR*) from (a) to the as-grown PL reference (solid lines): R_{pAg} – protected silver coated with unetched DBR, $R_{por\text{-}DBR}$ – uncoated area with etched porous-DBR, $R_{pAg+por\text{-}DBR}$ – coated with protected silver and etched porous-DBR area. For illustration, expected *PLR* ratio for combined effect of protected silver and porous-DBR is given by $R_{pAg} * R_{por\text{-}DBR}$ (dashed line). PL enhancement given as a ratio between measured PL data and the expected $R_{pAg\_por\text{-}DBR}/(R_{pAg} * R_{por\text{-}DBR})$ (dotted line). Arrows show the locations of the QW PL peak emission and the Tamm plasmon due to silver layer (Ag–Tamm) respectively, and grey bar shows the reflectivity stop-band for the porous-DBR from measurements. Inset shows the QW emission region in detail.

recorded PL spectra display two main features: first, a characteristic peak at around 363 nm (3.42 eV) from the GaN band edge excitonic emission, and second, a much stronger emission band at around 480–500 nm (2.58–2.48 eV) associated with InGaN QW emission, see for example Fig. 2(a)–(d). It is necessary to consider influence from different elements in the structure on the QW emission separately, before discussing the spectra of the final silver coated structure with etched porous-DBR. To visualise these changes, the averaged PL spectra for each sample area are first plotted in the Fig. 3(a) and then as a PL intensity ratio, *PLR* vs wavelength, shown by solid lines in Fig. 3(b). The latter was obtained by dividing the averaged PL spectrum from each of the three processed sample areas by a reference, which is given by the average PL from the as-grown region. The resulting *PLR* values reflect the effect of the processing

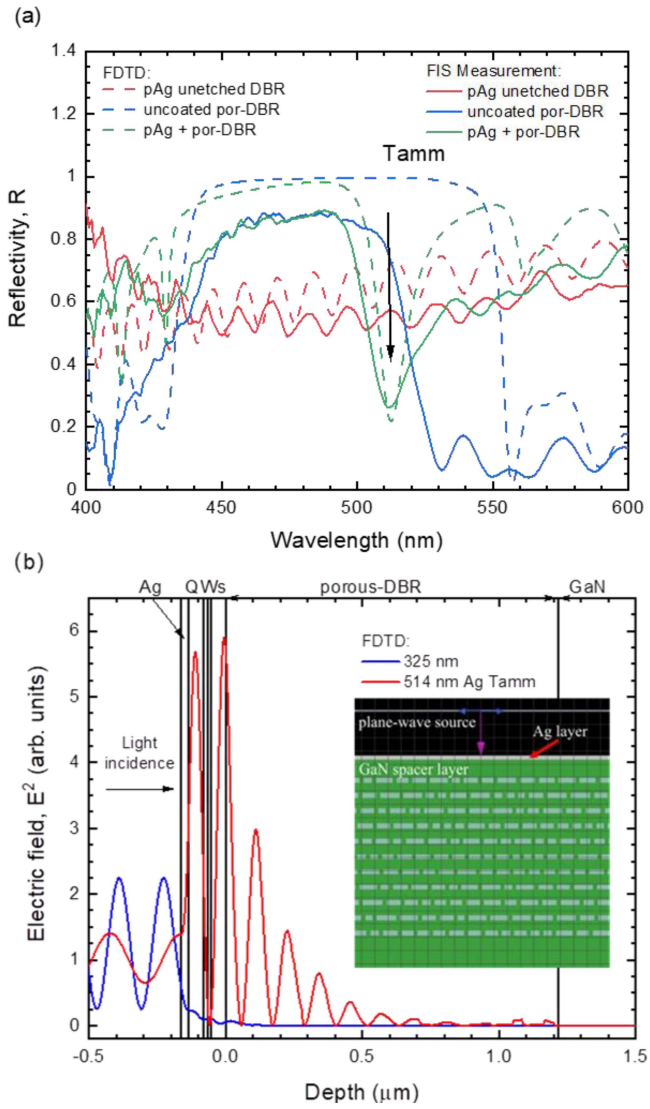

Fig. 4. (a) Reflectivity of the sample in the normal incidence versus wavelength from Fourier imaging spectroscopy (FIS) measurements (solid lines) and FDTD simulations (dashed lines) for different sample areas. (b) Calculated by FDTD light intensity as electric field E^2 versus depth in the sample with the silver porous-DBR microcavity for two different wavelength 325 nm (excitation) and 514 nm (Tamm plasmon). Arrow shows light incidence direction in the simulation. Locations of silver layer, InGaN QWs, GaN porous-DBR region and bottom GaN are shown. Inset shows details of porous-DBR and silver layer cavity model used in FDTD simulations.

step on PL emission and values below 1 indicate intensity signal has been decreased compared to the as-grown reference, and vice versa for the values above 1. To understand the origin and relative intensities of different peaks in the spectrum it is important to consider optical properties of the structure. Namely, the absorption/penetration depth of the excitation and reflectivity of different interfaces vs wavelength in this structure. To aid description of the optical properties of the structure the data from the FIS reflectivity measurements are plotted in the Fig. 4(a) for normal to the surface light propagation direction (solid lines) in the region of 400–600 nm. Results of FDTD simulations of the normal sample reflectivity, R vs wavelength for as-grown and processed sample areas are given in the Fig. 4(a) (dashed lines). The simulated light intensity as electrical field, E^2 profile vs depth in the micro-cavity at two different wavelengths is plotted in the Fig. 4(b) together with the sample geometry used for FDTD simulations, which are described in our previous work [11]. Since penetration depth of the 325 nm excitation light is only around 80 nm in the GaN [24], the 362 nm GaN band edge emission peak is originating mainly from the top 54 nm of GaN layer covering the QWs, see Fig. 1(b). Such shallow penetration depth of excitation results in the QW emission being dominated by the emission of the top 1.5–2 QWs only, see Fig. 1(b). It is also possible that some photoexcited carries from the top GaN barrier layer are diffusing into the top quantum well and contributing to the emission. The emitted 480–500 nm blue light from the InGaN quantum wells is, however, able to travel through the whole structure and is reflected at various interfaces creating Fabry-Pérot (FP) interference fringes observed in both PL and reflectivity spectra. Note, closer spacing between FP interference fringes indicates a larger thickness of the optical cavity and vice versa, see PL and reflectivity spectra, see Figs. 2 and 4.

A. *As-Grown Region*

Fig. 2(a) shows the typical photoluminescence signal with GaN band-edge related and QW emission peaks in the as-grown uncoated unetched samples. The QW emission peak is located around 483 nm (2.57 eV) and is broad (22 nm/100 meV FWHM). This peak also displays strong FP interference fringes due to multiple reflections between cavity interfaces, in this case formed by the top air/GaN and bottom GaN/sapphire interfaces (around 2.7 μm in total, see Fig. 1). There are some minor variations of the QW intensity from different locations in the as-grown area, mainly due to small changes in the FP interference conditions.

B. *Effect of Protected Silver Coating With no Porous-DBR*

Introduction of the protected Ag layer coating with thickness of 25 nm is decreasing the observed PL signal, compared with as-grown sample, see Fig. 2(a) and (b). The QW peak wavelength remains largely unchanged in these areas, and is centered around 483 nm, with FP fringes resembling those in as-grown material. While silver is generally reflective down to NUV wavelengths, its reflectivity dips at the 325 nm excitation wavelength [27], [28] and due to small thickness, a significant portion of the 325 nm light can penetrate into the structure and excite the PL in the GaN and QWs regions. The emitted blue light in the region of 480–500 nm is then additionally attenuated by a top silver later, before being collected by a microscope. To simplify considerations, we assume that top silver layer itself plays a role of a semi-transparent mirror for this area of the sample, i.e., reducing the intensity of the PL signal overall due to reflection/absorption and other interactions [26] are neglected. This reduction is approximately by a factor of 4–5 in the QW emission region, as seen by the *PLR* values plotted in the Fig. 3(b).

C. Effect of Porous-DBR Without Coating

Introduction of the porous-DBR increases the detected PL signal from the QWs, see Fig. 2(c). This happens mainly as a result of the QW emission being reflected upwards by the porous-DBR layer, which improves the light collection efficiency of the QW emission. The strain modification [29] in the layers after etching of the porous-DBR is very minor and can be neglected, as could be seen by a negligible shift of band edge emission from top GaN layer, see Fig. 3(a). The porous-DBR has also no effect on the excitation as most of the UV light as absorbed in the top cavity region, see Fig. 4(b). The lack of, or greatly enhanced spacing between FP fringes observed in the QW emission spectrum from the uncoated area with porous-DBR seen in Fig. 2(c) suggests that the effective optical cavity length is much less than it was in the as-grown area. This is consistent with porous-DBR forming a micro-cavity with the top air/GaN surface. The reflectivity stop-band due to the porous-DBR is measured to occur between 450 and 510 nm, given by $R > 0.8$, which is broadly consistent with the FDTD simulated result as shown in Fig. 4(a). The discrepancy between measurements and simulations can be explained here by additional scattering losses and oversimplification of the porous-DBR structure in the simulation, see Fig. 4(b) inset. From the *PLR* data in Fig. 3(b), most of the effect is observed on the high energy side of the QW emission peak at around 440–450 nm, where collected PL signal is enhanced around 4–5 times. The enhancement by porous-DBR for the main 480–490 nm QW emission is much more modest, on order of 1.2–1.3 times, see Fig. 3(b) inset. While the measured reflectivity of porous-DBR is over 80%, the lack of significant enhancement for the peak QW region and larger effect for high energies suggest that QW operates at near saturation point for its ground state emission and some re-absorption of light in the QWs might also occur. One has to note, the peak wavelength for the QW emission from this area is not significantly affected relative to the as-grown area, it is centered around 483 nm and there are no significant changes to the width of the QW emission peak or FP interference fringes.

D. Effect of Silver and Porous-DBR Micro-Cavity

Areas with micro-cavity formed by the protected silver layer and GaN/porous-GaN DBR mirrors result in an increased QW emission, though nominally the QW PL intensity does not significantly exceed ones from the uncoated as-grown region or just with porous-DBR, see Fig. 3(a). The *PLR* data for this area in the Fig. 3(b) shows an ∼1.25x increase of the signal for the 490–500 nm band above the one observed in the as-grown sample. Despite this small *PLR* value, the enhancement of the photoluminescence itself is much stronger and will be discussed separately below. Additionally, the peak of the QW emission is now red-shifted to around 493 nm (2.51 eV) for an averaged PL spectrum in Fig. 3(a), however the various spectra recorded over this area in Fig. 2(d) suggest a bimodal deconvolution of the QW PL with peaks at around 490 nm and 500 nm, respectively. The average full width of half maximum (FWHM) of the emission peak is also decreased to approx. 16 nm (82 meV), compared with the spectra from other regions, see Figs. 2 and 3(a).

Determining the PL signal enhancement factor is not straightforward for this structure. In the absence of any enhancement effects due to micro-cavity, we expect the effect on the PL signal to be simply a combination of the semi-transparent silver mirror effect (discussed in section B) and enhanced reflectivity of the porous-DBR (discussed in section C), which is shown by *PLR* data of these areas in Fig. 3(b). The following will describe this procedure. As effect of silver layer on the observed PL intensity is given by a factor of $R_{pAg} = \mathrm{PL_{pAg}/PL_{as\text{-}grown}}$ and porous-DBR by a factor of $R_{por\text{-}DBR} = \mathrm{PL_{por\text{-}DBR}/PL_{as\text{-}grown}}$, hence the expected combined effect of these two factors can be approximated as $R_{pAg} \times R_{por\text{-}DBR}$, shown by the dashed line in the Fig. 3(b). Further, the expected PL spectrum can be then obtained from the PL for as-grown area by multiplying it with the $R_{pAg} \times R_{por\text{-}DBR}$ product, given by dashed line in Fig. 3(a). For our case, since the effect of porous-DBR in the 480–500 nm QW PL region is very small (see Fig. 3(b) inset), the expected QW PL signal should be only slightly higher than the PL from pAg-coated region, in absence of any cavity enhancement effects. In reality, the measured PL from the micro-cavity area is much stronger than this expected one.

Hence, for the areas coated with protected silver and etched porous-DBR we define the figure of merit for micro-cavity enhancement factor via the ratio between the measured signal, $\mathrm{PL_{pAg+por\text{-}DBR}}$ to the expected level of signal, which is given as discussed by $\mathrm{PL_{as\text{-}grown}} \times R_{pAg} \times R_{por\text{-}DBR}$. In the absence of any enhancement effects from the hybrid micro-cavity resonances there should be no or very little difference between these two signals, i.e., ratio of 1 is expected for such case.

The resulting enhancement is shown by a dotted line in Fig. 3(b) as $R_{pAg\_por\text{-}DBR}/(R_{pAg} \times R_{por\text{-}DBR})$ obtained from averaged spectral data for each region. The resulting peak enhancement of the QW emission due to the hybrid micro-cavity effect at around 8.5 times occurs in the region 490–500 nm. The enhancement drops then to only ∼2× for the 480 nm and 514 nm wavelengths of QW and Tamm resonance, respectively, see Fig. 3(b). This effect can be explained by means of the Tamm plasmon mode resonance which exists for the light propagating at or very close to normal to the cavity interfaces. This mode can be understood as a combined effect of the metal plasmon due to silver coating layer on top of GaN semiconductor, and the optical micro-cavity resonance created by the porous-DBR and the top surface [14], [11], [17], [25]. The Tamm mode resonance can be experimentally observed as a reflectivity dip in the cavity stop-band, see Fig. 4(a). In an ideal condition, the maximum enhancement is expected to occur at the wavelength of the Tamm resonance, and ideally this should be co-located with the emission peak of the QW region. For the 25 nm silver thickness used here, the Tamm resonance is predicted and measured at around 514 nm, given in Fig. 4(a). As the as-grown QW PL emission is centered at 483 nm wavelength, so the maximum 8.5x enhancement observed here is due to only a partial overlap between Tamm mode and the QW emission, i.e., experimentally observed in between these two values, see Figs. 2(d) and 3(b). Further, the strength of the QW peak in the micro-cavity sample is reducing the more the emission maxima is red-shifted to 500 nm, this increases the energetic overlap with the Tamm

mode, but decreases an overlap with optical transitions available in a QW at this wavelength, and vice versa, see Fig. 2(d). Although this detuning of the Tamm and QW energies is preventing this structure from operating efficiently and to show any optically pumped lasing (excitation power dependence is not shown here), this behaviour is beneficial for our study, as it allows for a clearer separation of effects due to Tamm resonance and any other processes affecting peak emission in the QW. Note, much stronger variations of the QW PL intensity and peak wavelength are observed across the micro-cavity area of the sample, than in other areas (Fig. 2). This is likely due to some inhomogeneity in the porous-DBR etching and silver coating, i.e., micro-cavity properties across the area.

The mechanism of signal enhancement here is similar to other optically excited metal plasmon interactions with light emitters, where the enhancement is achieved via change in the local electric field/density in the region of QW. This is so-called the Purcell effect [21], [26], affecting radiative carrier lifetimes and most likely competing with various de-localisation effects for electrons and holes due to potential fluctuations of the InGaN QW energy bands, which occur due to In composition and well thickness variations, piezoelectric fields, etc. [26]. This is consistent with the picture from FDTD simulations, showing electric field distribution created by a Tamm resonance with the light inside the cavity, see Fig. 4(b). This results in a relatively narrow regions of very high electric field extending deep under the silver contact, locations of which will be sensitive to the silver layer and cavity thicknesses and corresponding reflectivities. The simulation predicts only a partial spatial overlap of Tamm plasmon electric field and the QW region at 514 nm wavelength, see Fig. 4(b). Therefore, in addition to the energy match between the QW peak and Tamm plasmon, the active emitting region needs to be co-located with one of the maximums of the Tamm electric field distribution inside the micro-cavity, for its emission to be enhanced significantly and to increase oscillator strength. These two conditions are essential for further optimisation of this type of the devices [17], [25].

Silver and other metals, such as gold, aluminium and alloys can be used to tune the Tamm mode in the visible region from the blue to NUV and yellow parts of the spectrum. Equally, the GaN porous-DBR can be modified via change in the layer structure and etching conditions to create strong reflectivity stop-bands across the same regions with reflectivity approaching 100% [17]. This allows for the exploitation of such plasmonic micro-cavities not only for the blue-green region, as demonstrated here, but also for the green-yellow InGaN QW emitting devices based on conventional c-plane GaN epitaxy or non/semi-polar GaN growth. Improving efficiency for green-yellow InGaN devices is of great importance,[1] as internal quantum efficiency drops significantly with increase of In composition above 15% in the QW, and Tamm plasmon resonances can mitigate some of these effects and create efficient structures even on polar c-plane GaN material, as discussed here. Another advantage of Tamm/porous-DBR micro-cavity is that it is easier to maintain electrical conductivity through this structure, compared with dielectric DBRs, as Tamm metal layer can also aid electrical contacts formation in the electrically pumped vertically emitting devices.

IV. Conclusion

In summary, we have successfully demonstrated the route for photoluminescence output enhancement in the vertical InGaN MQW emitting structure, containing a hybrid micro-cavity based on GaN/porous-GaN DBR and metal silver layer. The effect of enhancement is attributed to the Tamm plasmon resonance in such a cavity, and an InGaN QW PL enhancement of 8.5 times was observed compared with expected effect of silver layer and porous-DBR alone. The micro-cavity emission peak was red-shifted towards the Tamm plasmon resonance at 514 nm and there was some QW emission peak narrowing. This structure can be further optimised and utilised to create optically and electrically pumped surface emitting diodes based on GaN, e.g., VCSELs, and can lead to efficient bright InGaN LEDs and laser devices not only in blue, but also in the green-yellow parts of the spectrum, which suffer from dramatic quantum efficiency droop.

Acknowledgment

The authors would like to thank Ye Tian, Peter Fletcher, and Tao Wang at Centre for GaN Materials and Devices, Department of Electronic and Electrical Engineering, University of Sheffield, Mappin Street, Sheffield S1 3JD, United Kingdom for the growth of the InGaN/GaN samples in this study.[1]

References

[1] S. Nakamura and M. R. Krames, "History of gallium–Nitride-based light-emitting diodes for illumination," *Proc. IEEE*, vol. 101, no. 10, pp. 2211–2220, Oct. 2013, doi: 10.1109/JPROC.2013.2274929.

[2] K. Ding, V. Avrutin, N. Izyumskaya, Ü. Özgür, and H. Morkoç, "Micro-leds, a manufacturability perspective," *Appl. Sci.*, vol. 9, no. 6, Mar. 2019, Art. no. 1206, doi: 10.3390/app9061206.M.

[3] L. Zhao, C. Liu, and K. Wang, "Progress of GaN-based optoelectronic devices integrated with optical resonances," *Small*, vol. 18, no. 14, Apr. 2022, Art. no. 2106757, doi: 10.1002/smll.202106757.

[4] T. Hamaguchi, M Tanaka, and H. Nakajima, "A review on the latest progress of visible GaN-based VCSELs with lateral confinement by curved dielectric DBR reflector and boron ion implantation," *Jpn. J. Appl. Phys.*, vol. 58, 2019, Art. no. SC0806, doi: 10.7567/1347-4065/ab0f21.

[5] J. Han, "(Invited) the progress and outlook of GaN laser devices," in *Proc. Electrochem. Soc. Meeting Abstr.*, 2018, vol. MA2018-02, Paper 1154, doi: 10.1149/MA2018-02/34/1154.

[6] C. Zhang et al., "Mesoporous GaN for photonic engineering – Highly reflective mirrors as an example," *ACS Photon.*, vol. 2, no. 7, pp. 980–986, Jul. 2015, doi: 10.1021/acsphotonics.5b00216.

[7] P. Fletcher et al., "Optical characterisation of InGaN-based microdisk arrays with nanoporous GaN/GaN DBRS," *J. Phys. D: Appl. Phys.*, vol. 55, no. 46, Sep. 2022, Art. no. 464001, doi: 10.1088/1361-6463/ac8fa0.

[8] C.-J. Wang, Y. Ke, G.-Y. Shiu, Y.-Y. Chen, Y.-S. Lin, and C.-F. L. H.Chen, "InGaN resonant-cavity light-emitting diodes with porous and dielectric reflectors," *Appl. Sci.*, vol. 11, no. 1, Dec. 2021, Art. no. 8, doi: 10.3390/app11010008.

[9] Z. L. Xie et al., "High reflectivity AlGaN/AlN DBR mirrors grown by MOCVD," *J. Cryst. Growth*, vol. 298, pp. 691–694, Jan. 2017, doi: 10.1016/j.jcrysgro.2006.10.216.

[10] Y. Tian et al., "Nearly lattice-matched GaN distributed Bragg reflectors with enhanced performance," *Materials*, vol. 15, no. 10, May 2022, Art. no. 3536, doi: 10.3390/ma15103536.

[11] J. R. Pugh et al., "A Tamm plasmon-porous GaN distributed Bragg reflector cavity," *J. Opt.*, vol. 23, no. 3, Feb. 2021, Art. no. 035033, doi: 10.1088/2040-8986/abdccb.

[1]Data supporting this study are openly available from IEEE DataPort at doi: 10.21227/e2gy-vw70.

[12] I. Tamm, "O vozmozhnoi sviazi elektronov na poverkhnostiakh kristalla," *Zh. Eksp. Teor. Fiz.*, vol. 3, pp. 34–35, 1933.
[13] M. Kaliteevski et al., "Tamm plasmon-polaritons: Possible electromagnetic states at the interface of a metal and a dielectric Bragg mirror," *Phys. Rev.*, vol. 76, Oct. 2007, Art. no. 165415, doi: 10.1103/PhysRevB.76.165415.
[14] M. Parker, E. Harbord, A. Young, P. Androvitsaneas, J. Rarity, and R. Oulton, "Tamm plasmons for efficient interaction of telecom wavelength photons and quantum dots," *IET Optoelectron*, vol. 12, no. 1, pp. 11–14, Feb. 2018, doi: 10.1049/iet-opt.2017.0076.
[15] M. Parker et al., "Telecommunication wavelength confined Tamm plasmon structures containing InAs/GaAs quantum dot emitters at room temperature," *Phys. Rev. B*, vol. 100, no. 16, Oct. 2019, Art. no. 165306, doi: 10.1103/PhysRevB.100.165306.
[16] E. Harbord et al., "Confined Tamm plasmon optical states coupled to a photoconductive detector," *Appl. Phys. Lett.*, vol. 115, no. 17, Oct. 2019, Art. no. 171101, doi: 10.1063/1.5121597.
[17] G. Lheureux et al., "Tamm plasmons in metal/nanoporous GaN distributed Bragg reflector cavities for active and passive optoelectronics," *Opt. Exp.*, vol. 28, no. 12, pp. 17934–17943, Jun. 2020, doi: 10.1364/OE.392546.
[18] M. E. Sasin et al., "Tamm plasmon polaritons: Slow and spatially compact light," *Appl. Phys. Lett.*, vol. 92, no. 25, Jun. 2008, Art. no. 251112, doi: 10.1063/1.2952486.
[19] C. Symonds et al., "Confined Tamm plasmon lasers," *Nano Lett.*, vol. 13, no. 7, pp. 3179–3184, Jun. 2013, doi: 10.1021/nl401210b.
[20] P. Das, S. Mukherjee, M. Wan, S. K. Ray, and S. B. N. Bhaktha, "Optical Tamm state aided room-temperature amplified spontaneous emission from carbon quantum dots embedded one-dimensional photonic crystals," *J. Phys. D, Appl. Phys.*, vol. 52, no. 3, Nov. 2019, Art. no. 035102, doi: 10.1088/1361-6463/aae9c7.
[21] Y.-D. Zheng, F.-A. Xiao, W.-J. Liu, and X.-L. Hu, "Purcell effect and light extraction of Tamm-plasmon-cavity green light-emitting diodes," *Opt. Exp.*, vol. 27, no. 14, pp. 30852–30863, Oct. 2019, doi: 10.1364/OE.27.030852.
[22] Y. Hou, Z. Ahmed Syed, L. Jiu, J. Bai, and T. Wang, "Porosity-enhanced solar powered hydrogen generation in GaN photoelectrodes," *Appl. Phys. Lett.*, vol. 111, no. 20, Nov. 2017, Art. no. 203901, doi: 10.1063/1.5001938.
[23] T. Zhu et al., "Wafer-scale fabrication of non-polar mesoporous GaN distributed Bragg reflectors via electrochemical porosification," *Sci. Rep.*, vol. 7, Mar. 2017, Art. no. 45344, doi: 10.1038/srep45344.
[24] S. Adachi, *Optical Constants of Crystalline and Amorphous Semiconductors: Numerical Data and Graphical Information*. Berlin, Germany: Springer, 1999, doi: 10.1007/978-1-4615-5247-5.
[25] P. S. Maji, G. Banerjee, and S. Acharyya, "Design rules for optical Tamm plasmon refractive index sensor based on porous-GaN," *Opt. Quant. Electron.*, vol. 54, Aug. 2022, Art. no. 623, doi: 10.1007/s11082-022-04054-3.
[26] P. Renwick, H. Tang, Q. Wang, R. Smith, and T. Wang, "Enhanced internal quantum efficiency of an InGaN/GaN quantum well as a function of silver thickness due to surface plasmon coupling," *Phys. Status Solidi C*, vol. 8, no. 7-8, pp. 2176–2178, Jun. 2011, doi: 10.1002/pssc.201001031.
[27] M.-M. Dujardin and M.-L. Theye, "Investigation of the optical properties of Ag by means of thin semi-transparent films," *J. Phys. Chem. Solids*, vol. 32, no. 9, pp. 2033–2044, 1971, doi: 10.1016/S0022-3697(71)80380-3.
[28] N. Ahmad, J. Stokes, N. A. Fox, M. Teng, and M. J. Cryan, "Ultra-thin metal films for enhanced solar absorption," *Nano Energy*, vol. 1, no. 6, pp. 777–782, Nov. 2012, doi: 10.1016/j.nanoen.2012.08.004.
[29] S. S. Pasayat et al., "Color-tunable $<10\,\mu$m square InGaN micro-leds on compliant GaN-on-porous-GaN pseudo-substrates," *Appl. Phys. Lett.*, vol. 117, no. 6, Aug. 2020, Art. no. 061105, doi: 10.1063/5.0011203.